ELSEVIER

International Journal of Mass Spectrometry 205 (2001) 325–330

International Journal of Mass Spectrometry

Role of morphology of D_2O ice (20–160 K) in low energy electron stimulated desorption of D^- and O^- anions, and x-ray photon stimulated desorption of D^+ cations

Michel Tronc[a,*], Roger Azria[b]

[a]*Laboratoire de Chimie Physique Matière et Rayonnement, Université Pierre et Marie Curie et CNRS UMR 7614, 11 Rue Pierre et Marie Curie—75231 Paris Cedex 05, France*

[b]*Laboratoire des Collisions Atomiques et Moléculaires, Université Paris-Sud et CNRS UMR 8625—Bt 351-91405 Orsay Cedex, France*

Received 17 February 2000; accepted 8 May 2000

Abstract

The low energy electron stimulated desorption yield of D^- anions in pure multilayer D_2O films, and of O^- in submonolayer O_2 covered D_2O films is strongly dependent on the D_2O condensation temperature (20–160 K) on Pt. Likewise the desorption of D^+ cations induced by oxygen 1*s* excitation to the ground state empty levels of D_2O depends on ice condensation temperature. These observations are connected with the morphology of ice films which are microporous and amorphous at $T <$ 90 K and crystalline at $T >$ 150 K. Moreover both the change of morphology and related adsorption capacity of ice films with condensation temperature are observed in situ with x-ray absorption spectroscopy. (Int J Mass Spectrom 205 (2001) 325–330)

Keywords: Desorption (ESD, PSD); Morphology; Ice

1. Introduction

Low energy electron attachment and inner-shell excitation are powerful techniques to study empty levels in molecules and their dynamics, and a correlation has been established between the resonance structures that dominate near edge x-ray absorption spectra (NEXAFS) and low energy electron scattering [electron transmission, resonant vibrational excitation and dissociative electron attachment (DEA)] [1,2]. The dominant role of localized molecular resonances (transient anion states and core hole excited states) has been extended to molecular solids [3–5], but for condensed molecules both electron stimulated desorption (ESD) and photon stimulated desorption (PSD) processes are strongly influenced by the environment [6,7]. It was for example found that at low electron energies where ESD proceeds via DEA [8] anion desorption can be modified by the presence of the dense surrounding medium because of mechanisms such as resonant coupling, charge transfer, electron energy loss, or ion–molecule interaction [9] and the self-trapping of electrons [10]. Moreover recent studies of D^- ESD [11] and D^+ PSD [12,13] from condensed D_2O and, of O^- anions from O_2 covered multilayers D_2O films [14] show that temperature and

* Corresponding author.

Dedicated to Professor Aleksandar Stamatovic on the occasion of his 60th birthday.

1387-3806/01/$20.00
PII S1387-3806(00)00269-4

morphology (crystallinity, microporosity, roughness, permeability, surface area) strongly influence the dissociation and desorption processes [6] as well as adsorption capacity and chemical reactivity of ice surfaces [7]. Although a great abundance of experimental and theoretical works is devoted to condensation, growth, nucleation, structure, surface properties of ice [15,16, and references therein] very little is known on the specific role of ice temperature and morphology on ESD and PSD and their role in atmospheric and interstellar photochemistry processes. In the following we present some aspects of the temperature and morphology of ice in cation and anion desorption for pure multilayer condensed films of ice and for oxygen covered ice films.

2. Morphology and adsorption of D_2O ice films

Fig. 1 shows oxygen 1*s* excitation spectra [total electron yield (TEY)] for D_2O water at different temperatures: 300 K [Fig. 1(a)] for gas phase molecules [17], 150 K [Fig. 1(b)] for crystalline hexagonal ice and 20 K [Fig. 1(c)] for amorphous porous ice, respectively. The spectra for ice have been deconvoluted and interpreted following the assignment of the isolated water molecule. The first two peaks in ice are attributed to mixed valence-Rydberg levels $4a_1^*/3s$ and $2b_2^*/3p$, respectively, higher energy peaks to oxygen *np* Rydberg levels. We observe that condensation has little effect on the first two peaks which have comparable relative intensity and width in condensed phase and for isolated molecules. The 0.9 eV width [full width at half maximum (FWHM)] is probably the Franck-Condon width of the strongly dissociating state. The small (0.8 eV) blueshift of these lines may be related to the four-coordinated oxygens in the bulk ice. By contrast, excited Rydberg levels in ice are strongly broadened and their intensities are enhanced, probably because repulsive interactions with neighbouring molecules localise the diffuse Rydbergs in the molecular core resulting in a shift to higher energy and an increase in the oscillator strength for the corresponding transitions compared to the gas phase. Such localisation is expected to depend

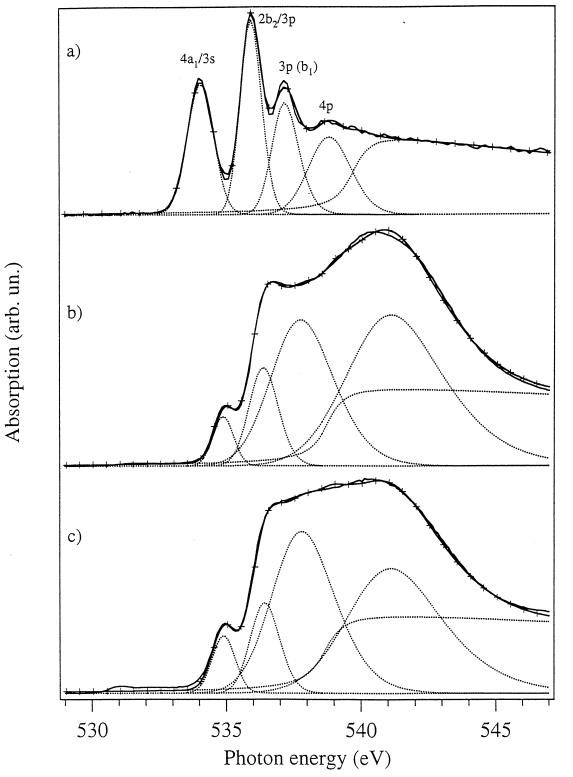

Fig. 1. Oxygen 1s photoabsorption spectrum of D_2O at different temperatures: (a) $T = 300$ K (gas phase [17]), (b) $T = 150$ K (100 ML crystalline hexagonal ice), (c) $T = 20$ K (100 ML microporous amorphous ice).

on local symmetry and on distances between surrounding molecules, which may explain the difference between NEXAFS of amorphous and crystalline ice below the O 1*s* ionisation threshold, particularly for the transition assigned to a $3p(b_1)$ level at 537.9 eV (Fig. 1) which is antisymmetric relative to the molecular plane. Moreover multiple scattering structures (not shown) in the O 1*s* ionisation continuum are clearly observed for crystalline ice but are blurred out with the structural phase transition crystalline → amorphous. Thus it appears that NEXAFS spectroscopy is not only very sensitive to the environment of the excited atom, but also to very small modifications of local electronic and geometric structure in a bulk condensate; it can probably be used to follow phase transition.

Brunauer, Emmett, Teller (BET) analysis of gas adsorption isotherms has shown the specific surface

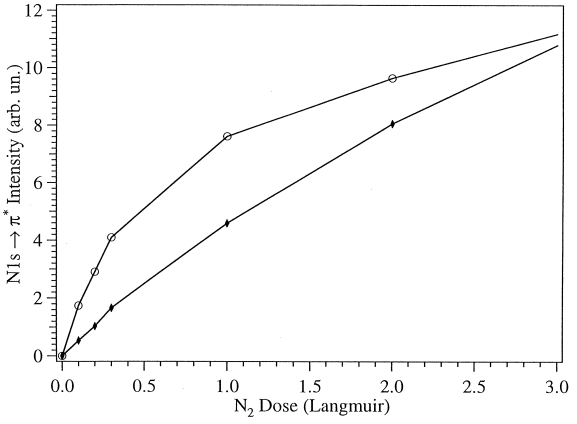

Fig. 2. Adsorption of molecular nitrogen N_2 at 20 K vs. the N_2 exposition dose on 100 ML of D_2O ice condensed at (a) 150 K and (b) 20 K, measured from the N 1*s* → π^* resonance intensity.

area of ice to be strongly dependent on condensation temperature [18,19] and on the total mass of ice deposited [20]. In the present experiment we have exposed crystalline and porous amorphous ice to variable doses of molecular nitrogen and measured the quantity of molecules adsorbed versus the N_2 exposition dose from the intensity of the strong N 1*s* → π^* resonance around 400 eV. The results are shown in Fig. 2. For crystalline ice, adsorption is linear with the exposition dose, the N_2 molecules condense at the ice surface. For amorphous porous ice, with more adsorption sites for a given surface, adsorption is strong for low (<0.5 L) exposition dose because the N_2 molecules diffuse and coat the connected micropores. For higher doses (3 L), adsorption on porous amorphous ice approaches the crystalline ice adsorption regime.

3. D^- ESD from condensed D_2O films

The energy dependence of the D^- ESD yield from D_2O ice shows three peaks at about 7, 9, and 11 eV. These peaks are associated with DEA processes via the $^2B_1$, $^2A_1$, and $^2B_2$ D_2O^-* resonance states respectively [11,21]. As shown in Fig. 3. from Simpson and co-workers the energy dependence of the D^- signal changes with temperature for both porous

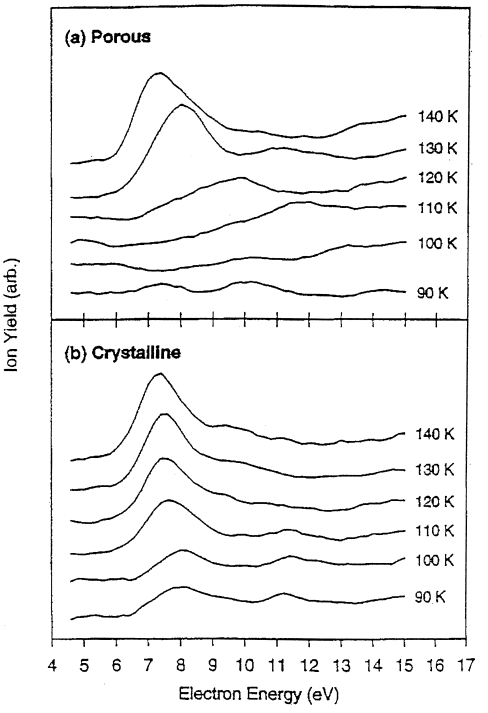

Fig. 3. D^- signal vs. incident electron energy collected at various temperatures (a) from 60 bilayers of porous amorphous ice films grown at 90 K, and (b) from 60 bilayers of crystalline ice films grown at 155 K. (from Simpson et al. [11]).

amorphous and crystalline D_2O ice [11]. In these spectra the D_2O films were grown at 90 K (porous amorphous) or 155 K (crystalline) and then heated or cooled to the temperature indicated in the figure for data collection. We see from these figures that the DEA resonance energies shift to lower energies and that the desorption D^- yield rises significantly when the temperature is increased except at the structural phase transition temperatures. Moreover a comparison of Fig. 3(a) and (b) shows that the temperatures at which these changes occur, depend on the morphology of the ice film. These effects have been associated [11] with variations of the work function at the lowest temperatures, with the condensation-induced perturbation of the $4a_1^*/3s$ orbital, which is doubly occupied in the three low lying DEA resonance states, and with changes in the hydrogen bonding network [11] as the temperature and morphology of the condensed films are changed.

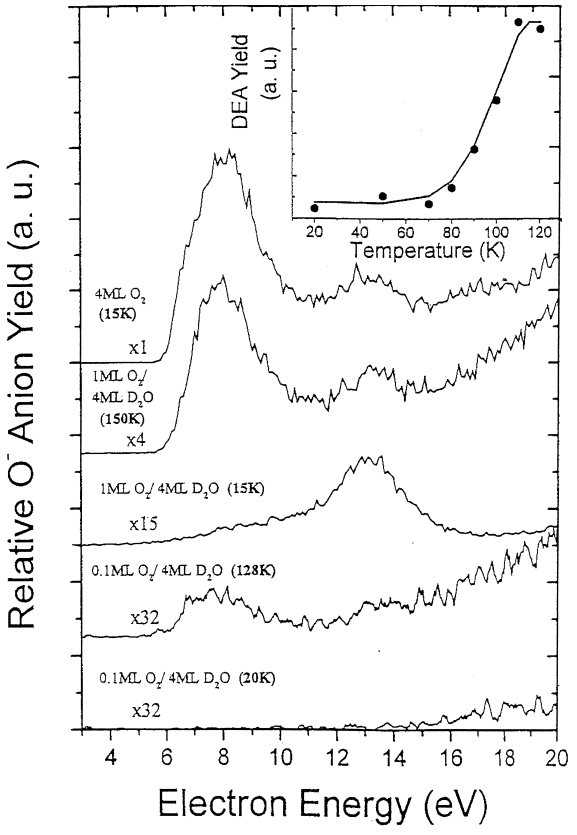

Fig. 4. O^- ESD yields from 1 ML O_2 and from 0.1 ML O_2 condensed on 4 ML D_2O films grown at temperatures of 15, 20, 128, and 150 K. The inset shows the magnitude of O^- ESD signal as a function of D_2O spacer condensation temperature integrated between 6 and 10 eV, for 0.3 ML O_2 condensed on 8 ML D_2O.

4. O^- ESD from O_2 covered multilayer condensed D_2O

O^- ESD yield from pure condensed O_2 [22,23] (Fig. 4) shows two structures in the 6–10 eV energy range associated respectively with DEA processes via the gas phase $^2\Pi_u$ and gas phase forbidden $^2\Sigma_g^+$ O_2^{-*} resonance states, and a third structure around 13 eV ascribed to dissociation of a transient $^2\Sigma^+$ anion state (the g/u assignment of which is undetermined). Moreover it has been shown that kinetic energy (KE) distributions of the desorbing O^- anions are broad, with KE extending up to 3 and to 5 eV for the 8 and 13 eV O^- yield peaks, respectively. We also see from Fig. 4, (1) that when 0.1 ML of O_2 is condensed on 4 ML D_2O films grown at 20 K (amorphous porous film), the O^- ESD signal is strongly suppressed below 15 eV, (2) that the O^- resonant signal is clearly observed for 0.1 ML and 1 ML of O_2 condensed on 4 ML D_2O grown at 128 K (amorphous non porous) and 150 K (crystalline), with features comparable with that of pure O_2 films, (3) that the O^- resonant signal is observed for 1 ML of O_2 condensed on 4 ML of amorphous porous D_2O (grown at 15 K) but with the relative intensities of the 8 and 13 eV peaks reversed from the pure O_2 or previous cases.

These observations are interpreted in terms of morphology of the D_2O films. When 0.1 ML of O_2 is deposited onto the porous amorphous 4 ML D_2O spacer film, O_2 molecules diffuse into the pores toward the Pt substrate. Then in addition to O^- anion collisions with surrounding molecules before reaching the surface, two other effects may contribute to suppression of the DEA O^- desorbing signal, namely quenching of the O_2^- resonance states by the metal [24] and an increase of polarization energy due to the stronger image force potential near the Pt substrate [24]. As the amount of deposited O_2 increases, so does the O^- signal, but since these ions suffer collisions as they diffuse though the D_2O spacer, O^- ions with higher KE (i.e. formed around 13 eV incident energy) have a higher probability to emerge into vacuum. This explains the reversed relative intensities of the 8 and 13 eV peaks when 1 ML of O_2 is deposited on 4 ML D_2O condensed at 15 K. When D_2O is condensed at 128 or 150 K the O_2^- resonance states are clearly observed. At these temperatures the D_2O spacer layer is in a non porous amorphous and crystalline phase, so that O_2 molecules are unable to diffuse through the D_2O layer and remain on the D_2O surface. In these cases, O^- desorption arises from the surface giving O^- yield functions similar to those obtained in pure O_2. The temperature dependence of the O^- DEA signal integrated between 6 and 10 eV is shown in the inset of Fig. 4 for 0.3 ML O_2 condensed on 8 ML D_2O. It indicates that O_2 diffusion through the D_2O spacer layer is increasingly inhibited as the temperature of the D_2O film condensation rises from 80 to 120 K. Above 120 K the O^- signal remains constant. These results are understood to arise from a

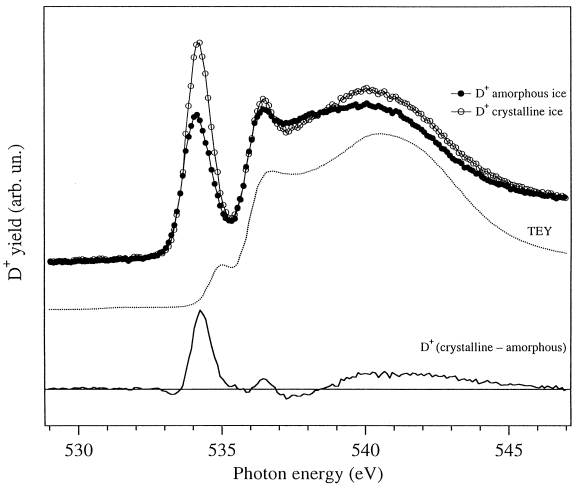

Fig. 5. D^+ PSD yield from 100 ML of D_2O ice films condensed at 150 K (open circles) and 20 K (solid circles). The continuous line is the difference D^+ (crystalline) − D^+ (amorphous). The dotted line is the O 1*s* NEXAFS for crystalline ice.

reduction of the number or size of the micropores in the D_2O film, with increasing temperature, which restricts O_2 diffusion.

5. D^+ PSD from D_2O ice films

Fig. 5 shows the total D^+ PSD yields as a function of photon energy at glancing light incidence, in the region of oxygen *K* shell for thick (100 ML) amorphous porous (20 K) and crystalline (150 K) D_2O ice films. The more relevant observations are the following (1) the yield of desorbing D^+ ions for crystalline ice is higher than for porous amorphous ice as can be seen in the difference curve (Fig. 5), and this difference is more pronounced for the threshold D^+ peak at 534 eV, (2) this threshold D^+ peak is shifted to lower energy (0.6 eV) and is strongly enhanced compared with the photoabsorption threshold peak, while broader structures between 535 and 540 eV parallel roughly those in the total electron yield. From saturation effects and polarization dependence it has previously been shown that the D^+ threshold peak is a fast direct PSD process and higher structures result from both PSD and x-ray induced electron stimulated desorption by Auger, secondary, and photo electrons [25]. As ion desorption is a surface sensitive process, the low energy shift of the D^+ threshold peak compared with the TEY may result from a different electronic structure of surface relaxed D_2O molecules with a lower oxygen coordination number (2 or 3) than in the bulk (4), and less hydrogen bonding, so that bulk-ice energy levels (both occupied and unoccupied) may not accurately represent the energy states at the desorption sites at (near) the surface. This redshift of the excitation energy of the D^+ peak is in line with the calculated variation for O 1*s* excitation energies in gaseous H_2O as a function of symmetrical stretching of the O–H bond [26]. The modification of the Rydberg-valence mixing and antibonding character of the $4a_1^*/3s$ orbital with condensation and core ionisation may furthermore explain the high dissociation probability of this state to produce D^+ ions. The increased lifetime of core hole excited states for surface molecules, together with the existence of different hydrogen bonding and O–D dangling bonds depending on the morphology of ice and hence on condensation temperature are probably active factors in the D^+ desorption yield, and in the difference between amorphous and crystalline ice films. Clearly x-ray induced photon stimulated ion desorption (XPSID) is a powerful technique to study the surface reactivity of ice as it is sensitive to electronic and atomic structure of the first layer at the surface.

6. Conclusion

Low energy electron attachment, and inner shell excitation spectroscopies probe ground-state empty levels in molecules and produce short-lived resonance states. The dynamics of these states observed via ESD of anions (D^-, O^-) and PSD of cations (D^+) is strongly dependent on the morphology (temperature) of condensed D_2O films which may have a strong influence on heterogeneous catalytic reactions appearing on icy surfaces of polar stratospheric clouds and of dusts or particles in the interstellar medium. NEXAFS and XPSID are powerful techniques to study bulk phase transition and surface reactivity of adsorbates, respectively.

Acknowledgements

The authors would like to thank Y. Le Coat, F. Bournel, C. Laffon, and Ph. Parent for their active and fruitful participation to this work. This study was supported by the CNRS and the University Paris VI and XI.

References

[1] A. Benitez, J.M. Moore, J.A. Tossell, J. Chem. Phys. 88 (1988) 6691.
[2] F. Guillot, C. Dezarnaud-Dandine, M. Tronc, A. Modelli, A. Lisini, P. Decleva, G. Fronzini, Chem. Phys. 205 (1996) 359.
[3] L. Sanche, M. Michaud, Phys. Rev B 30 (1984) 6078.
[4] L. Sanche, Phys. Rev. Lett. 53 (1984) 1638.
[5] J. Stöhr, in NEXAFS Spectroscopy, Springer Series in Surface Sciences Vol. 25, Springer, Berlin, 1992.
[6] M.N. Hedhili, L. Parenteau, M. A. Huels, R. Azria, M. Tronc, L. Sanche, J. Chem. Phys. 107 (1997) 7577.
[7] J.E. Schaff, J.T. Roberts, J. Chem. Phys. 100 (1996) 14151.
[8] L. Sanche, J. Phys. B: At. Mol. Opt. Phys. 23 (1990) 1597.
[9] M.A. Huels, L. Parenteau, L. Sanche, J. Chem. Phys. 100 (1994) 3940.
[10] Q.B. Lu, T.E. Madey, Phys. Rev. Lett. 82 (1999) 4122.
[11] W.C. Simpson, M.T. Sieger, T.M. Orlando, L. Parenteau, K. Nagesha, L. Sanche, J. Chem. Phys. 107 (1997) 8668.
[12] H.T. Siegler, N.C. Simpson, T.M. Orlando, Phys. Rev. B 56 (1997) 4925.
[13] M. Tronc, F. Bournel, C. Laffon, P. Parent, Chem. Phys. Lett., in press.
[14] R. Azria, Y. Le Coat, M. Lachgar, M. Tronc, L. Parenteau, L. Sanche, Surf. Sci. 436 (1999) 671.
[15] Physics and Chemistry of Ice, J. Phys. Chem. B 101 (1997).
[16] P.A. Thiel, T.E. Madey, Surf. Sci. Rep. 7 (1987) 211.
[17] G.R. Wright, C.E. Brion, J. Electron Spectrosc. 4 (1974) 25.
[18] K.P. Stevenson, G.A. Kimmel, Z. Donalek, R.C. Smith, B.D. Kay, Science 283 (1999) 1505.
[19] E. Mayer, R. Pletzer, Nature 319 (1986) 298.
[20] M.T. Leu, L.F. Kaiser, R.S. Timonen, J. Phys. Chem. B 101 (1997) 6259.
[21] M. Tronc, R. Azria, Y. Le Coat, E. Illenberger, J. Phys. Chem. 100 (1986) 14745.
[22] R. Azria, Y. Le Coat, J.P. Ziesell, J.P. Guillotin, B. Mharzi, M. Tronc, Chem. Phys. Lett. 220 (1994) 417.
[23] M.A. Huels, L. Parenteau, M. Michaud, L. Sanche, Phys. Rev. A 51 (1995) 337.
[24] H. Sambe, D.E. Ramaker, L. Parenteau, L. Sanche, Chem. Phys. Lett. 59 (1987) 236.
[25] D. Coulman, A. Puschman, U. Höfer, H.P. Steinrüch, W. Wurth, P. Feulner, A. Menzel, J. Chem. Phys. 93 (1990) 58.
[26] J. Schrimer, A.B. Trofimov, R.J. Randall, J. Feldhaus, A.M. Bradshaw, Y. Ma, C.T. Chen, F. Sette, Phys. Rev. A 47 (1993) 1136.